Electronic Supplementary Information

Durable and Recyclable Biomimetic Glycol Lignin/Polyolefin Compounds for a Circular Economy

Jonathon Tanks, Kenji Tamura, Kimiyoshi Naito, Thi Thi Nge, Tatsuhiko Yamada

---

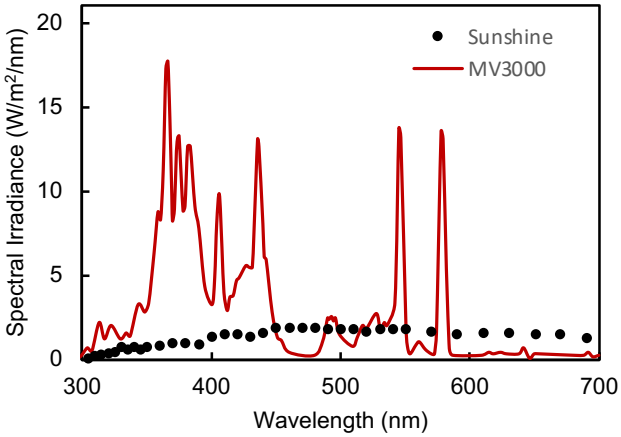

Figure S1. Irradiance spectrum of MV3000 lamp used for UV irradiation (according to manufacturer).

Figure S2. Overview of the degradation/recycling flow used in this study. Pellets are inserted into a stainless steel mesh holder with a gap roughly the width of a pellet, which ensures fairly uniform exposure by limiting overlap and crowding. After 300 MJ/m^2 of UV irradiation (equivalent to at least 1 year of sunlight), the pellets are carefully removed and either injected molded as-is or subjected to further processing before molding.

FTIR analysis indicates that ester bonds are formed between glycol-modified lignin (GL) and maleic-grafted PP. A shift in the carbonyl region from 1775 cm^{-1} to 1733 cm^{-1} signifies the formation of esters and carboxylic acids, and an increase in -COOH (3450 cm^{-1}) relative to -OH (3300 cm^{-1}).

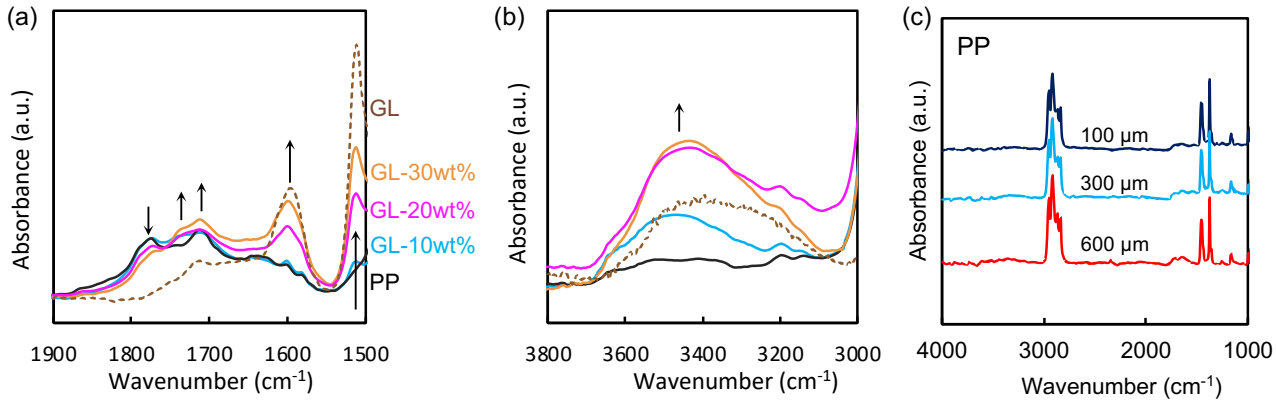

Figure S3. FTIR spectra of GL/PP blends in the (a) carbonyl region and (b) hydroxyl region. (c) Through-thickness FTIR spectra of neat PP reference specimen taken with IR-microscope.

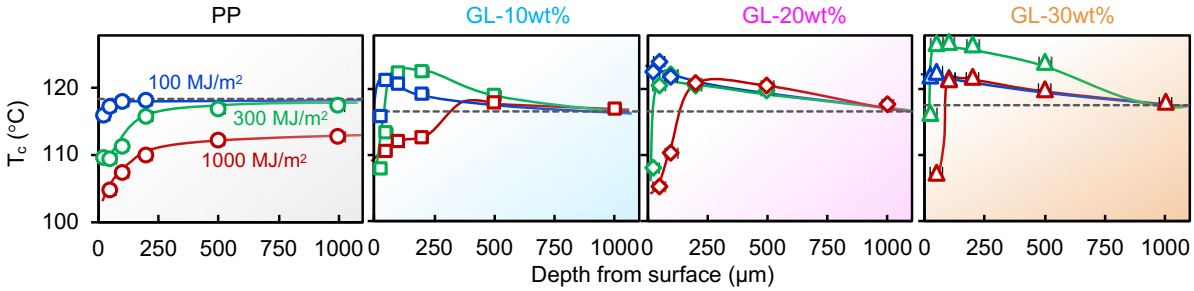

Figure S4. Crystallization temperature (*Tc*) measured though the specimen thickness at different UV irradiation energies for different GL/PP blends.

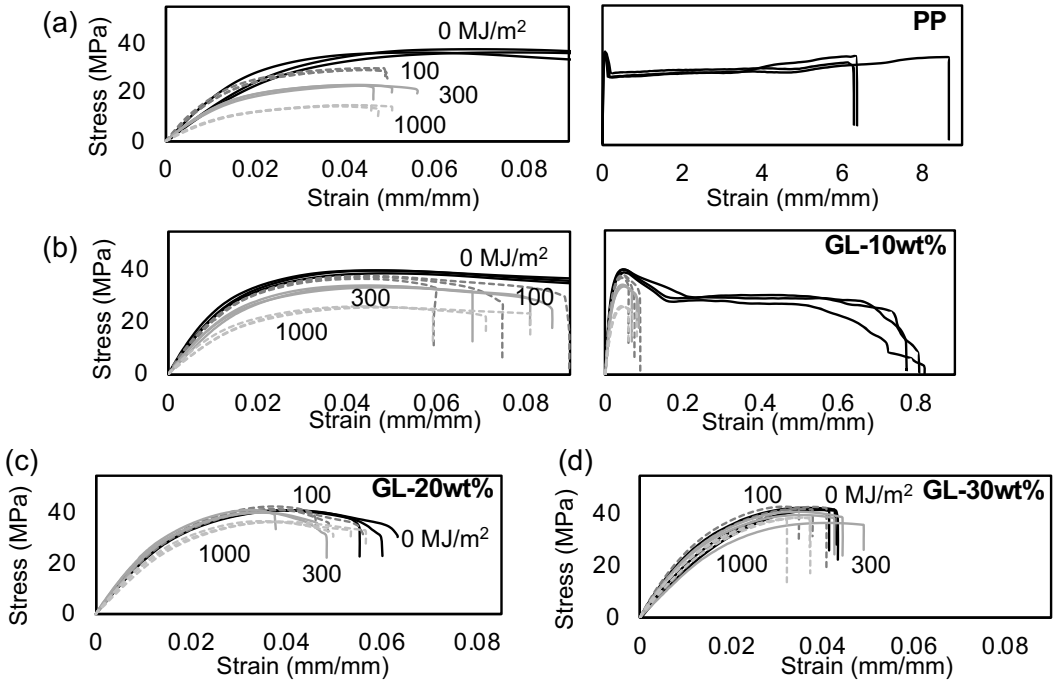

Figure S5. Tensile stress-strain curves for (a) neat PP, (b) GL-10wt%, (c) GL-20wt%, and (d) GL-30wt%.

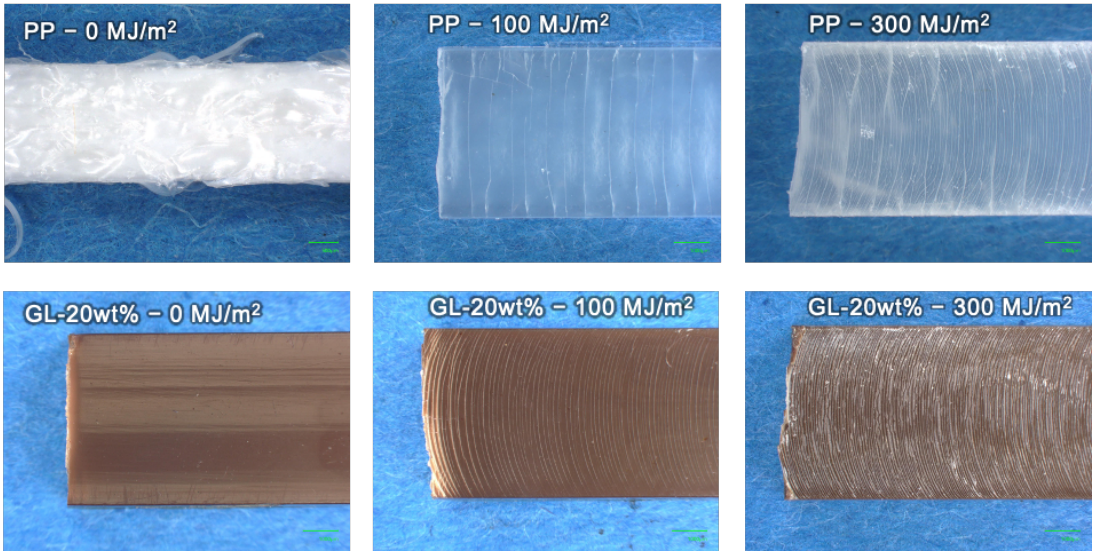

Figure S6. Photographs of neat PP and GL-20wt% specimen surfaces after tensile testing in the reference/initial state (before irradiation) and after different UV irradiation doses. Note that pre-exposure neat PP shows high elongation and strain-induced crystallization, making it appear white and fibrous.

Linear elastic fracture mechanics (LEFM) assumes that the total energy of a system takes the form of (i) potential energy stored in elastic strain, and (ii) the free energy of a new crack surface. Furthermore, if the yielding region ahead of the crack tip is sufficiently small relative to the size of the body, the stress field near the crack tip can be expressed by Westergaard solution [S1]:

$$\sigma_{yy} = \frac{\sigma_\infty}{\sqrt{1-\left(\frac{a}{x}\right)^2}} \tag{S1}$$

where σ_{yy} is the stress perpendicular to the crack faces, σ_∞ is the far-field (equilibrium) stress in the bulk, a is the crack length (labeled d_c in the manuscript for surface crack depth), and x is the position along the crack growth direction; i.e., the crack tip is located at $a = x$, and σ_{yy} approaches σ_∞ when x grows very large relative to a. This relation is shown for different arbitrary crack lengths in Figure S7(a). The nominal strength σ_N (i.e., the failure stress for a material with surface flaws) can be described by Irwin's relation [S1]:

$$\sigma_N = \begin{cases} \sigma_0 & (a < a_{cr}) \\ \dfrac{K_{IC}}{\sqrt{\pi a}} & (a \geq a_{cr}) \end{cases} \tag{S2}$$

where σ_0 is the material's intrinsic tensile strength in the pristine state, K_{IC} is the critical fracture toughness above which a crack grows, and a_{cr} is a critical crack depth above which the nominal strength transitions from intrinsic material strength to crack-dominated failure. This model is illustrated in Figure S7(b) for a general case. The measured crack depths after different irradiation energies are shown in Figure S8, and LEFM predictions of nominal strength using several values of K_{IC} are compared in Figure S9.

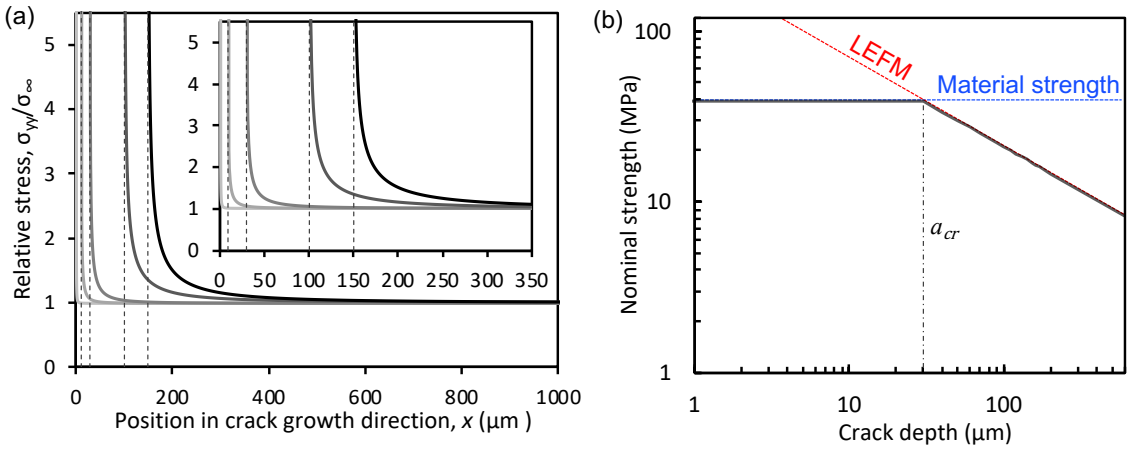

Figure S7. (a) Westergaard solution for stress field around a crack, and (b) Schematic of transition from inherent material strength to LEFM-dominated failure stress.

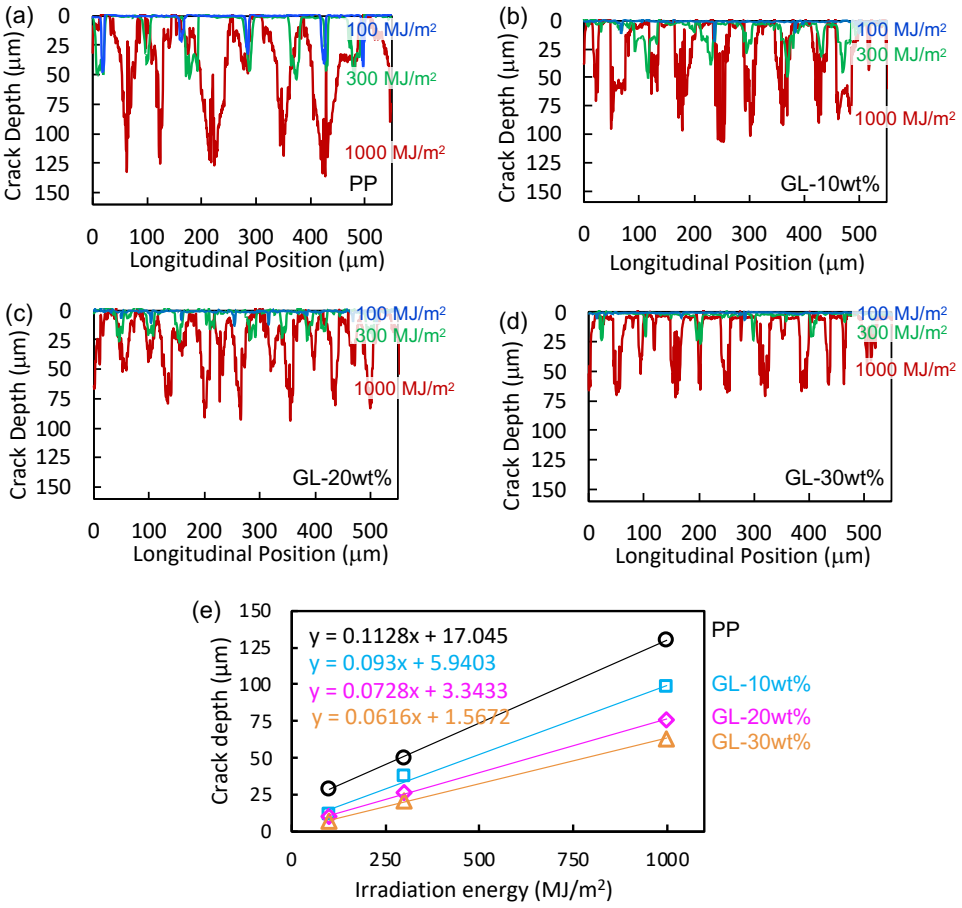

Figure S8. Surface crack depths (measured by LSM) after irradiation for (a) neat PP, (b) GL-10wt%, (c) GL-20wt%, and (d) GL-30wt%. (e) Crack growth rates with respect to irradiation energy for different GL blends.

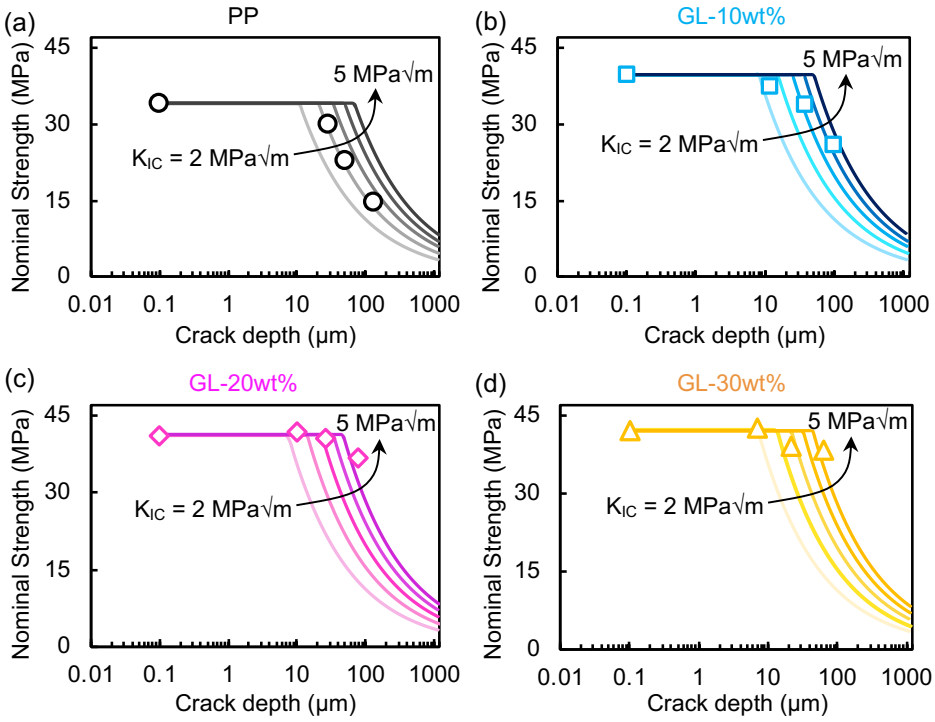

Figure S9. LEFM predictions of nominal tensile strength using different values of K_{IC} for (a) neat PP, (b) GL-10wt%, (c) GL-20wt%, and (d) GL-30wt%.

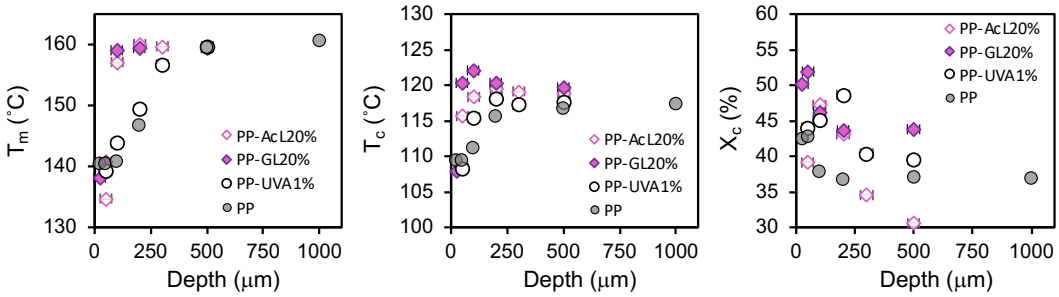

Figure S10. Melting temperature (T_m), crystallization temperature (Tc), and crystallinity (X_c) measured though the specimen thickness for (a) UVA-1wt%, and (b) AcL-20wt%, after 300 MJ/m^2 of irradiation.

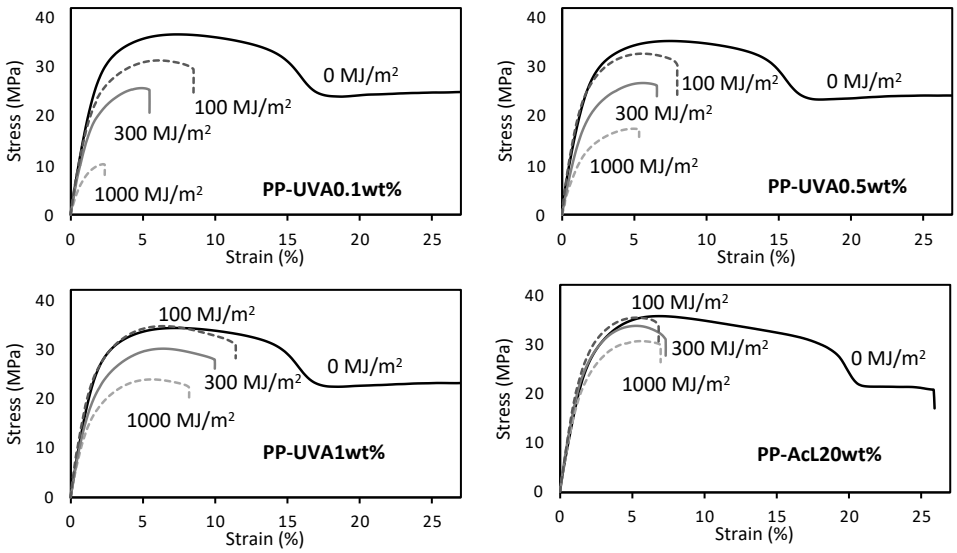

Figure S11. Tensile stress-strain curves for (a) UVA-0.1wt%, (b) UVA-0.5wt%, (c) UVA-1wt%, and (d) AcL-20wt%.

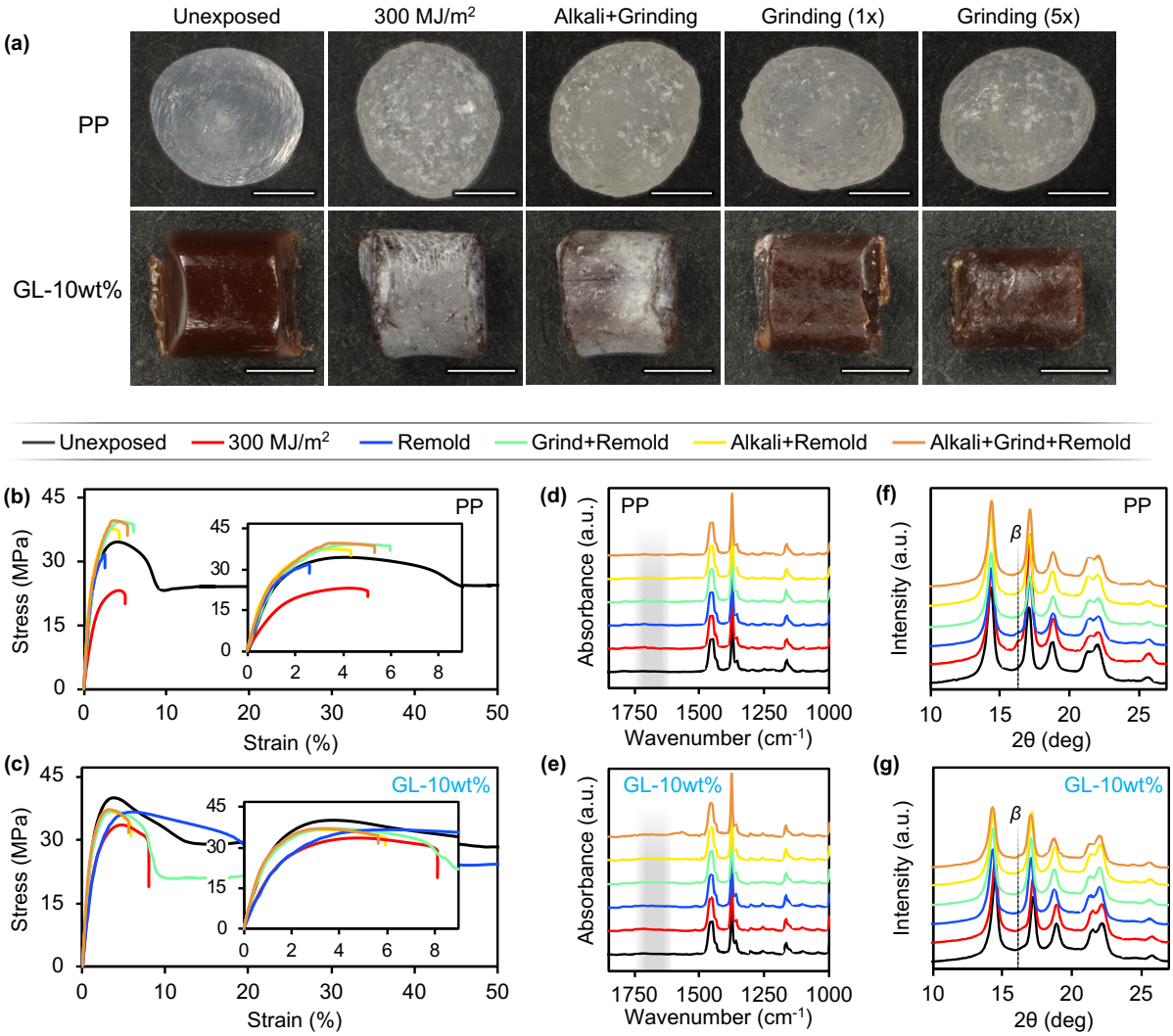

Figure S12. Summary of neat PP and GL-10wt% specimens subjected to various recycling protocols after 300 MJ/m^2 of irradiation: (a) Photographs of pellets in different conditions (scale bars are 1 mm). (b,c) Tensile behavior, (d,e) FTIR spectra, and (f,g) XRD patterns.

Supplementary References

S1. D. Taylor, P. Cornetti, N. Pugno, The fracture mechanics of finite crack extension, *Eng. Fract. Mech.*, 2005, **72**, 1021-1038.